Spin-orbit coupling controlled ground state in the Ir(V) perovskites A_2ScIrO_6 (A = Ba or Sr)

Paula Kayser, Brendan J. Kennedy* and Ben Ranjbar

School of Chemistry, The University of Sydney, Sydney, NSW 2006

Justin A. Kimpton

Australian Synchrotron, 800 Blackburn Road, Clayton, Victoria 3168, Australia

Maxim Avdeev

Australian Nuclear Science and Technology Organization, Lucas Heights, New South Wales, 2234, Australia

* E-Mail Brendan.Kennedy@Sydney.edu.au

Abstract

The structural and magnetic properties of the two Ir(V) perovskites Ba_2ScIrO_6 and Sr_2ScIrO_6 have been established. The structures were refined using a combined neutron and Synchrotron data set. At room temperature the former has a cubic structure in space group $Fm\bar{3}m$ a = 8.1450(3) Å and the latter is monoclinic in $P2_1/n$ with a = 5.6606(3) b= 5.6366(3) c = 7.9720(4) Å β = 89.977(5)°. Magnetization measurements show both oxides have magnetic moments close to zero as a consequence of strong spin-orbit coupling that results in a $J_{eff} \sim 0$ ground state. The distortion of the IrO_6 octahedra in Sr_2ScIrO_6 is insufficient to generate crystal field splitting strong enough to quench the spin orbit coupling.

Introduction

There is considerable current interest in the structures and properties of oxides containing 4*d* or 5*d* transition metals, reflecting the realization that these often display complex behavior associated with their large spin-orbit coupling (SOC). The magnitude of the SOC can be comparable to the intra-atomic Coulomb (U) exchange and crystal electric field interactions. That the delicate balance between the interactions drives complex magnetic and dielectric behavior in iridates is well illustrated in a number of Ir^{4+} ($5d^5$) iridates that have a J_{eff} = ½ ground state, following on from the report of a spin-orbital Mott insulating state in the layered iridate Sr_2IrO_4 [1, 2], and the giant magnetoelastic effect in $Ba_3BiIr_2O_9$ [3] The need to understand the intermediate regime is typified by the diverse range of properties found in double perovskites containing 4*d* and 5*d* ions, including high-temperature half-metallic ferrimagnetism [4], Mott insulating states [5, 6], complex geometric frustration [7-9] and other structurally selective magnetic states [10]. The factors controlling this complex array of ground states remains poorly understood.

In comparison to the Ir^{4+} perovskites, the Ir^{5+} ($5d^4$) perovskites are even less studied. In the absence of strong SOC Ir^{5+} is expected to have a S= 1 ground state with two unpaired electrons, whereas strong spin-orbit coupling will result in a nonmagnetic singlet J_{eff} = 0 ground state [11] (Fig. 1). In 1964 Katz and Ward [12] reported the synthesis of the Ir^{5+} double perovskite Ba_2ScIrO_6 which Thumm and co-workers identified as having a cubic structure.[13] Subsequently Wakeshima *et al.* [14] refined the structure of this using conventional X-ray diffraction data, along with that of the Sr analogue Sr_2ScIrO_6, and described both of these as having an ordered double perovskite-type structure with monoclinic symmetry. The term double perovskite is commonly used to describe oxides of the type $A_2BB'O_6$ where the two octahedrally coordinated *B*-type cations exhibit a rock-salt like ordering.[15, 16] Numerous examples of double perovskites have been described with crystal symmetries ranging from cubic ($Fm\bar{3}m$) to triclinic ($P\bar{1}$). Howard *et al.* have established the group theoretical relationship between the various double perovskite structures [17].

It is generally accepted that in iridates SOC is the critical energy scale for determining physical properties. However, recent studies of Ir perovskites including Sr_2YIrO_6 [18] and $Ba_3YIr_2O_9$ [19] have shown that distortion of the IrO_6 octahedra results in a splitting of the energy levels that is comparable to the SOC energy scales. The distortion of the IrO_6 octahedra is

influenced by both octahedral rotations and a Jahn-Teller distortion and can broaden the t_{2g} bandwidth so that this also can also influence the physical properties.

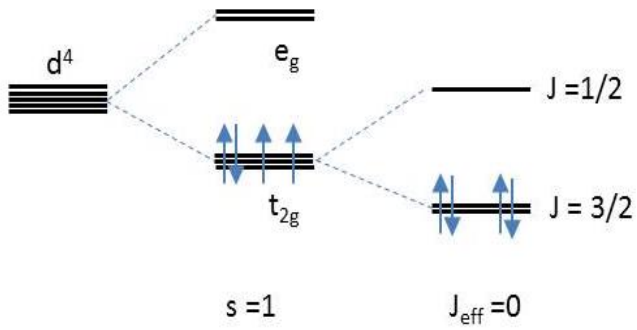

Figure 1. Ground state for a single Ir^{5+} ($5d^4$) ion. When the crystal field dominates a S = 1 ground state is expected and where strong spin orbit coupling dominates a J_{eff} = 0 ground state occurs.

Whilst iridium-based oxides remain relatively unexplored, it is evident that these often exhibit interesting physical properties. In the present paper we are concerned with the double perovskites A_2ScIrO_6 (A = Sr, Ba). In these oxides the size and charge difference between the Sc^{3+} and Ir^{5+} cations is sufficient to induce ordering of these resulting in interpenetrating FCC lattices. Consequently these double perovskites are geometrically frustrated magnetic materials and this adds another degree of complexity to these materials.[20, 21] Given the uncertainty regarding the precise structures of these oxides, and the possibility that strong SOC will drive unusual magnetic properties, we describe in this paper the structure of the two oxides A_2ScIrO_6 (A = Ba or Sr), determined using combined synchrotron X-ray and neutron studies, and their magnetic properties.

Experimental

Polycrystalline samples of Ba_2ScIrO_6 and Sr_2ScIrO_6 were prepared by solid state reaction. The appropriate stoichiometric mixture of $BaCO_3$ (Aldrich, 99.999 %), $SrCO_3$ (Aldrich, 99.99 %), Sc_2O_3 (Aldrich, 99.999 %) and Ir metal (Aithaca, 99.9 %) was weighed and finely mixed by

hand in an agate mortar. Prior to weighing the reagents, $BaCO_3$ and $SrCO_3$ were dried at 150 °C for 12 hours and Sc_2O_3 was heated at 1000 °C for 12 hours. The samples were placed in alumina crucibles and heated at 650 °C for 12 hours and 850 °C for 12 hours with intermediate regrinding. After mixing again, the samples were pressed into 20 mm pellets and heated in air at 1050 °C for 24 hours, 1200 °C for 72 hours and 1400 °C for 72 hours.

Synchrotron X-ray powder diffraction data were collected over the angular range $5 < 2\theta < 85°$, using X-rays of wavelength 0.82465 Å, as determined by a structural refinement of a diluted NIST SRM660b LaB_6 standard, on the powder diffractometer at BL-10 beamline of the Australian Synchrotron [22]. The samples were housed in 0.2 mm diameter capillaries that were rotated during the measurements. For the neutron diffraction measurements the sample was sealed in a 5 mm diameter vanadium can, to minimize the effect of neutron absorption by Ir, and the neutron powder diffraction data were obtained using the high resolution powder diffractometer Echidna at ANSTO's OPAL facility at Lucas Heights [23]. The wavelengths of the incident neutrons, obtained using (335) and (331) reflections of a germanium monochromator, were 1.6220 Å and 2.4395 Å, respectively, as determined using data collected for a certified NIST SRM660b LaB_6 standard. This instrument has a maximum resolution of $\Delta d/d \sim 1 \times 10^{-3}$. Structure refinements using the Rietveld method were carried out using the GSAS[24] program with the EXPGUI[25] front-end.

DC magnetic susceptibilities were measured using a Quantum Design PPMS9. Magnetic susceptibility data were collected from 300 K to 2 K using the vibrating sample magnetometer technique.

Results and Discussion

Crystallography

The powder X-ray diffraction patterns for both Ba_2ScIrO_6 and Sr_2ScIrO_6 showed a number of R-point reflections, in particular at $2\theta = 10.07°$ and 19.34°, that are indexed as (111) and (311) in a double perovskite unit cell, indicative of an ordered arrangement of the ScO_6 and IrO_6 octahedra. Essentially complete ordering of the Sc^{3+} and Ir^{5+} is expected due to the sizeable differences in valence state and ionic radius between Sc^{3+} (IR = 0.745 Å) and Ir^{5+} (IR = 0.57 Å)[26]. The S-XRD pattern of Ba_2ScIrO_6 showed no evidence for either splitting or anomalous broadening of the various reflections, and the pattern was reasonably well reproduced

by a cubic model in $Fm\bar{3}m$ with a = 8.1450(3) Å, although this model failed to fit a number of weak reflections, that could not be indexed to the monoclinic cell proposed by Wakeshima *et al*.[14] Examination of the difference profile suggested that the extra peaks were due to a small amount of a 6H-type phase. This hexagonal structure has been reported for the analogous ruthenium oxide Ba_2ScRuO_6.[27] Inclusion of this impurity phase leads to a significant improvement in the fit to the profiles and the final structure was refined against a combined X-ray and neutron data set. The weight fraction of the 6H phase was estimated to be 93.3(2)% based on Rietveld analysis of the room temperature S-XRD data. The Rietveld profiles are illustrated in Figure 2. Cooling the sample to 3 K did not result in the appearance of any additional reflections with the lattice contracting somewhat to 8.1393(1) Å. Evidently Ba_2ScIrO_6 does not show long range magnetic ordering. The Sc-O and Ir-O bond distances, at room temperature, are unexceptional being 2.0957(9) and 1.9768(8) Å respectively. The corresponding bond valence sums for Sc and Ir are 3.08 and 5.09 confirming that the Ir is pentavalent.

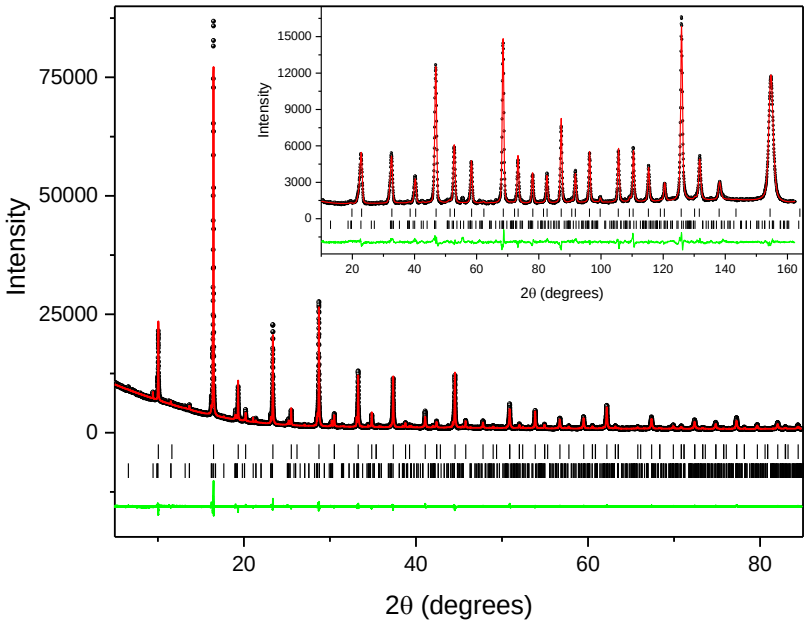

Figure 2. Synchrotron X-ray (main figure) and neutron (inset) Rietveld profiles for Ba_2ScIrO_6. The difference between the observed, indicated by the symbol, and calculated (solid line) profiles is given the lower trace. The upper set of markers is for the main cubic phase in $Fm\bar{3}m$ and the lower set for a 6H-type phase described in space group $P3m1$.

Table 1. Refined structural parameters for Ba_2ScIrO_6 at room temperature. The structure was refined in the cubic space group $Fm\bar{3}m$ using a combined S-XRD and ND data set.

Atom	*x*	*y*	*z*	Ui/Ue*100/ Å^3
Ba	¼	¼	¼	0.022(9)
Sc	0	0	0	0.183(18)
Ir	½	0	0	0.263(18)
O	0.25730(11)	0	0	0.38(9)

a = 8.1450(3) Å Vol = 540.35(4) Å^3 Sc-O 2.0957(9) Å BVS = 3.08 Ir-O 1.9768(9) Å BVS = 5.09 Neutron R_p 3.22 R_{wp} 4.22 S-XRD R_p 4.03 R_{wp} 5.80 χ^2 17.62

The S-XRD pattern of Sr_2ScIrO_6 exhibits noticeable splitting of a number of reflections, in particular both the basic (400) and (444) reflections are split indicating the symmetry is monoclinic. This suggests the structure is in either *I*2/*m* or *P*2$_1$/*n*. The neutron diffraction pattern for Sr_2ScIrO_6 revealed the presence of weak M-point reflections such as the 210/120 near 2θ = 37.5°. M-point reflections are indicative of in-phase tilting of the octahedra are arise from freezing of soft mode vibrations at the M-point (k = ½ ½ 0) of the Brillouin zone of the primitive cubic structure. R-point reflections, at (k = ½ ½ ½) are due to the rock-salt like ordering of the Sc and Ir cations and/or out-of-phase tilting of the octahedra. The superlattice reflections and peak splitting demonstrates the space group to be *P*2$_1$/*n* as assumed by Wakeshima *et al.*[14] That the M-point reflections were not apparent in the S-XRD profiles reflects both the small magnitude of the in-phase tilts and the dominance of the heavy Ir cations in X-ray diffraction. The structure of Sr_2ScIrO_6 was refined against a combined S-XRD and ND data set and these results are summarized in Table 2. The refined structure is essentially identical to that described recently for a sample prepared using wet chemical methods. [28] A feature of the structure is the relatively short Sc-O bond distances with the average Sc-O distance of 2.023 Å, being noticeably shorter than that observed in Ba_2ScIrO_6, Sc-O 2.096 Å and other *Ln*ScO_3 perovskites [29]. The average Sc-O bond distance in Sr_2ScOsO_6 is 2.054 Å.[30] The bond valence sum for the Sc cation, 3.65, in Sr_2ScIrO_6 is considerably greater than expected. This value is similar to that reported by Kayser *et al.*[28] although the bond valence sum for the Ir in Sr_2ScIrO_6 is consistent

with Ir^{5+} (4.98). The high Sc BVS is not a consequence of Sc-Ir anti-site disorder which was estimated to be 4(1)%, which is slightly more than that (9(1)%) described by Kayser *et al.*[28] The BVS for Sc in Sr_2ScOsO_6, 3.45, is also unusually high. Taylor *et al.*[30] noted that high pseudo symmetry in Sr_2ScOsO_6 required the use of bond distance constraints in their refinement against PND data; this is not an issue in the present case where the cell metric is determined by the high resolution synchrotron data.

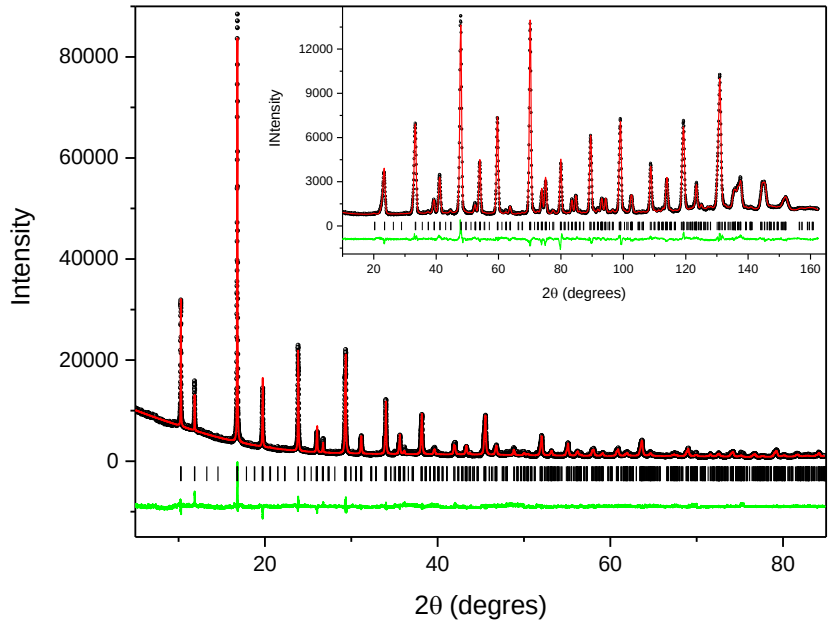

Figure 3. Synchrotron X-ray (main figure) and neutron (inset) Rietveld profiles for Sr_2ScIrO_6. The difference between the observed, indicated by the symbol, and calculated (solid line) profiles is given the lower trace. The markers show the position of all the allowed Bragg reflections in space group $P2_1/n$.

Whereas Ba_2ScIrO_6 is cubic in space group $Fm\bar{3}m$ and is described by the Glazer tilt notation $a^0a^0a^0$ the alternating ScO_6 and IrO_6 octahedra in monoclinic Sr_2ScIrO_6 are tilted in an antiphase manner along the (100) and (010) directions of the pseudocubic cell and tilted in phase along the (001) direction. This corresponds to the Glazer tilt system $a^-a^-c^+$, see Figure 4. The size of the in-phase tilt can be estimated from the Sc–O3– Ir bond angle ω as $\varphi = (180 - \omega)/2$. The observed value of 8.7° is somewhat smaller than we have found for Sr_2YIrO_6 which is 12.9°.

The presence of cooperative tilting in Sr_2ScIrO_6, but not in Ba_2ScIrO_6 reflects the need to optimize the smaller Sr–O bond lengths, and this is reflected in the tolerance factor for the two oxides t = 0.962 and 1.020 for A = Sr and Ba respectively. The Ir-O bond distances in Sr_2ScIrO_6 are approximately equal and the O-Ir-O bond angles are all near 90° giving quasi-regular octahedra. Cao has recently reported that the IrO_6 octahedra in the isostructural Y oxide, Sr_2YIrO_6 are compressed [18]; this is clearly not the case here.

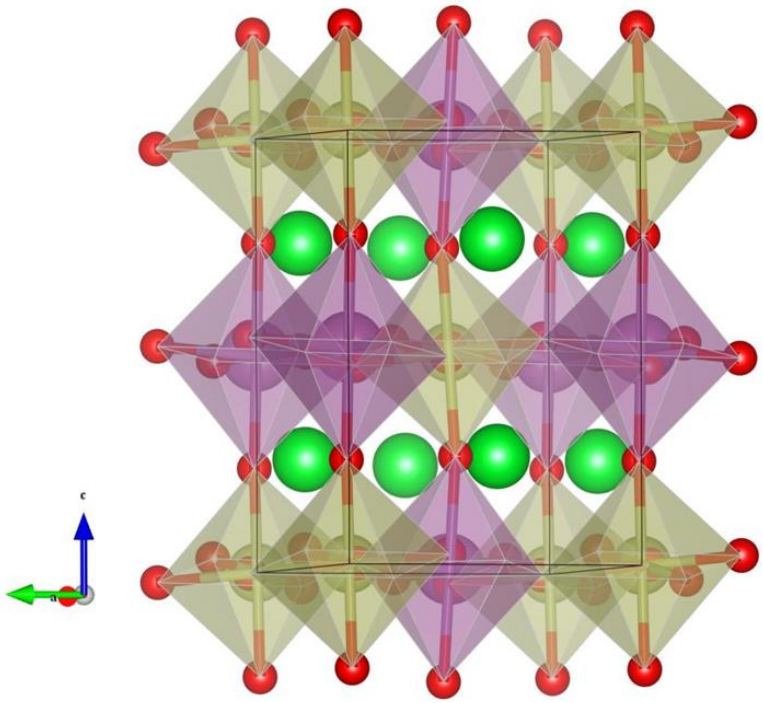

Figure 4. Representation of the monoclinic structure of Sr_2ScIrO_6 illustrating the tilting of the corner sharing ScO_6 and IrO_6 octahedra. The Sr cations (large green spheres) occupy the resulting 9-coordinate sites.

Table 2. Refined structural parameters for Sr_2ScIrO_6 at room temperature. The structure was refined in the monoclinic space group $P2_1/n$ using a combined S-XRD and ND data set.

Atom	x	y	z	Ui/Ue*100/ Å^3
Sr	0.0004(4)	0.4929(4)	0.2508(4)	0.69(2)
Sc	0	0	½	0.25(3)
Ir	0	0	0	0.02(1)
O1	0.0470(3)	-0.0014(6)	0.2492(8)	0.17(9)
O2	0.2417(6)	0.2555(6)	-0.0184(4)	1.3(4)
O3	0.2735(5)	0.7782(5)	-0.0279(4)	0.3(3)

a = 5.6606(3) *b*= 5.6366(3) *c* = 7.9720(4) Å β = 89.977(5)° V= 254.34(2) Å^3

Sc – O1 2.017(7) Sc-O2 2.014(4) Sc-O3 2.038(3) BVS = 3.65

Ir-O1 2.004(7) Ir-O2 1.992(4) and Ir-O3 2.003(3) BVS =4.98 Sc-O1-Ir 166.6(4)° Sc-O2-Ir 167.7(3)°.

Neutron R_p 3.85 R_{wp} 5.71 S-XRD R_p 5.71 R_{wp} 7.76 χ^2 14.11

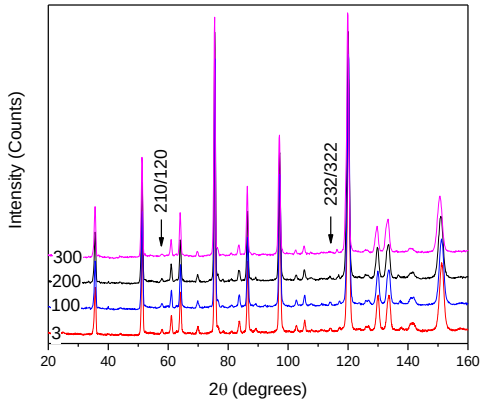

Figure 5. Observed neutron diffraction profiles of Sr_2ScIrO_6 measured upon cooling.

Figure 5 illustrates the changes in the NPD profiles as Sr_2ScIrO_6 is cooled to 3 K. The most significant changes are small increases in the intensities of selected superlattice reflections associated with a temperature induced increase in the magnitude of the octahedral tilting. The magnitude of the tilts can be estimated from the refined atomic coordinates [31, 32] and the in-phase tilt was observed to increases from 3.9 to 5.6° and the out-of-phase from 7.6 to 8.8° upon cooling

from room temperature to 3 K. These tilt angles are noticeably smaller than seen in Sr_2YIrO_6 where they are 11.4 and 7.8 ° respectively[33] which is consistent with the smaller radius of Sc^{3+} compared to that of Y^{3+}, 0.745 Å vs. 0.90 Å, respectively. There is no evidence for long range magnetic ordering or for a crystallographic phase transition.

The IrO_6 in Sr_2ScIrO_6 octahedron are remarkably regular at room temperature however these become slightly flattened upon cooling to 3 K with the bond distance between Ir and apical oxygen Ir-O1 (=1.954(12) Å) being slightly shorter than the in-plane Ir-O2 and Ir-O3 bond distances, 2.036(8) Å and 2.016(6) Å, respectively. Cooperative tilting of the corner sharing octahedra induces a distortion of the octahedra and it is likely that these changes simply reflect the increased magnitude of the tilts at low temperatures. Conversely the IrO_6 octahedra in Sr_2YIrO_6 are slightly elongated with bond distances of 1.960, 1.965 and 1.998 Å [8].

Magnetic Susceptibilities

The temperature dependence of the zero-field cooled (ZFC) magnetic susceptibilities (χ_m) for Ba_2ScIrO_6 and Sr_2ScIrO_6 are illustrated in Figure 6 and show no evidence for long range magnetic ordering down to 2 K. This is consistent with the NPD measurements described above. There is no significant divergence of the Field Cooled and ZFC susceptibilities. Critically there is no evidence for any magnetic impurities, the previous study of Sr_2ScIrO_6 showed clear evidence for the presence of a, weakly ferromagnetic, $Sr_3Ir_2O_7$ impurity [28, 34] which prevented analysis of the susceptibility data. As evident from Figure 6, the inverse susceptibility data do not obey the Curie-Weiss law. The observed behaviour is similar to that seen recently in the analogous Y containing oxides A_2YIrO_6 where the unusual behaviour was ascribed to a combination of strong SOC and a small amount of a paramagnetic phase[33]. In a cubic field Ir^{5+} is expected to have a low spin $t_{2g}^4 e_g^0$, (S = 1) configuration and hence is expected to be magnetic. The symmetry of the Ir cation in Sr_2ScIrO_6 is lower than cubic and while this will lift the degeneracy of the t_{2g} orbitals, it is not expected to result in a diamagnetic state. Strong SOC will split the t_{2g} into energetically lower 4 J_{eff} = 3/2 and higher 2 J_{eff} = ½ states. The J_{eff} = 3/2 band will be filled by the d^4 electrons resulting in the appearance of an electrically insulating J_{eff} = 0 singlet ground state (Fig. 1).

The temperature dependence of the magnetic susceptibilities was fitted to the equation:

$$\chi_{cal} = \left[(1-d) * \frac{C}{T-\theta} + TIP\right] + d * \left(\frac{0.375}{T}\right)$$

where C and θ are Curie and Weiss constants respectively, d indicates the amount of paramagnetic impurity and *TIP* is a temperature independent contribution to the magnetic susceptibility. The fitting suggested the samples contained ~ 0.1 (A = Sr) or 0.2 (A = Ba) % of an S = 1 impurity. It is speculated that this is associated with local disorder within the structure that is not evident from the diffraction studies.

The Weiss constant θ was found to be approximately zero for both oxides and that the TIP term was non-trivial ~ 5 x 10^{-4} emu mol^{-1}. This is similar to that estimated in the analogous Y containing oxides A_2YIrO_6. The effective magnetic moment per Ir is 0.16 μ_B/Ir in Sr_2ScIrO_6 and 0.39 μ_B/Ir for Ba_2ScIrO_6 which is much less that the value expected for a conventional S = 1 system (2.83 μ_β/Ir) demonstrating the ground state is dominated by strong SOC.

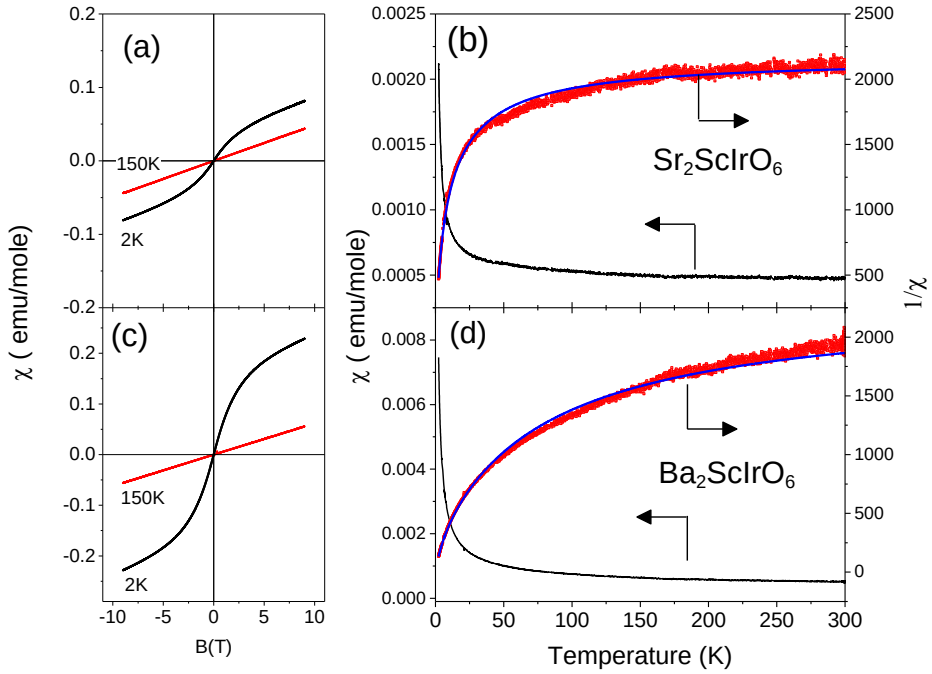

Figure 6. Isothermal magnetization (a) and (b) and temperature dependence of dependence of the magnetic susceptibilities (black lines) and inverse susceptibilities (red symbols) for Sr_2ScIrO_6 and Ba_2ScIrO_6 (c) and (d). The blue lines in (b) and (d) and the fits described in the text.

Finally it is informative to compare this pair of oxides to related oxides A_2YBO_6 and A_2ScBO_6 (A = Ba, Sr; B = Ru, Ir, Os) [18, 35, 36] where SOC is believed to be influential in establishing the ground state. As expected from the Goldschmidt tolerance factor reducing the size of the A-site cation from Ba to Sr reduces the symmetry, introducing cooperative tilting of the corner sharing octahedra, with the structure of the Sr oxides invariably being monoclinic in $P2_1/n$. Nevertheless as seen in the present study the magnetic ground states within the various Sr-Ba pairs are similar demonstrating that distortions of the shape and bond angles of the BO_6 octahedra are generally insufficient to generate crystal field splitting strong enough to quench the competing SOC. The present systems provide further evidence of this, as do the recent studies of the Y^{3+} analogues A_2YIrO_6. [11] In the d^3 case Sr_2ScOsO_6 there is evidence that SOC induced anisotropy in the ground state contributes to the relatively high T_N. It is possible that this is also significant in the isoelectronic $4d^3$ ruthenates. In situations where magnetic exchange between the transition metal is important, the electronic configuration of the non-magnetic B-site cation Sc^{3+} ($3d^0$) or Y^{3+} ($4d^0$) influences the overall magnetic exchange interactions.[37] This is evident in the Os containing oxides.

Experimentally it is clear that irrespective of the A-site cation (Sr or Ba) or non-magnetic B-site cation (Y or Sc) the Ir^{5+} containing double perovskites have a $J_{eff} \sim 0$ ground state. This is consistent with a simple point charge model which suggests that strong SOC interactions should cause Ir^{5+} to have paired spins ($J_{eff} \sim 0$) and therefore a net $\mu_{eff} \sim 0$. Nevertheless the oxides exhibit non-zero moments. The spatially extended 4d and 5d orbitals are expected to enhance the covalence of the B-O chemical bonds and this will be influenced by the choice of the A-site cation. Since the A–O interaction competes with the B-site ions for the O-2p(π) electrons, the stronger ionic character of the Ba^{2+}, relative to Sr^{2+}, makes it less competitive for the O-2p orbitals, which enhances the covalent admixture of O-2p(π) character into the primarily 4d-electron π^* bands. It is postulated that the covalence of the Ir-O bonds contributes to the observed non-zero magnetic moments.

Acknowledgments

This work was, in part, performed on the powder diffraction beamline at the Australian Synchrotron. BJK acknowledges the support of the Australian Research Council.

References

(1) Jackeli, G.; Khaliullin, G. Mott Insulators in the Strong Spin-Orbit Coupling Limit: From Heisenberg to a Quantum Compass and Kitaev Models. *Phys. Rev. Lett.,* **2009,** 102, 017205.

(2) Watanabe, H.; Shirakawa, T.; Yunoki, S. Monte Carlo Study of an Unconventional Superconducting Phase in Iridium Oxide J(eff)=1/2 Mott Insulators Induced by Carrier Doping. *Phys. Rev. Lett,* **2013,** 110, 027002.

(3) Miiller, W.; Avdeev, M.; Zhou, Q. D.; Kennedy, B. J.; Sharma, N.; Kutteh, R.; Kearley, G. J.; Schmid, S.; Knight, K. S.; Blanchard, P. E. R.; Ling, C. D. Giant Magnetoelastic Effect at the Opening of a Spin-Gap in $Ba_3BiIr_2O_9$. *J. Amer. Chem. Soc,* **2012,** 134, 3265-3270.

(4) Kobayashi, K. L.; Kimura, T.; Sawada, H.; Terakura, K.; Tokura, Y. Room-temperature magnetoresistance in an oxide material with an ordered double-perovskite structure. *Nature,* **1998,** 395, 677-680.

(5) Erickson, A. S.; Misra, S.; Miller, G. J.; Gupta, R. R.; Schlesinger, Z.; Harrison, W. A.; Kim, J. M.; Fisher, I. R. Ferromagnetism in the Mott insulator Ba_2NaOsO_6. *Phys. Rev. Lett.,* **2007,** 99, 016404.

(6) Gangopadhyay, S.; Pickett, W. E. Spin-orbit coupling, strong correlation, and insulator-metal transitions: The J(eff)=3/2 ferromagnetic Dirac-Mott insulator Ba_2NaOsO_6. *Phys. Rev. B,* **2015,** 91, 045133.

(7) Aharen, T.; Greedan, J. E.; Ning, F.; Imai, T.; Michaelis, V.; Kroeker, S.; Zhou, H.; Wiebe, C. R.; Cranswick, L. M. D. Magnetic properties of the S=3/2 geometrically frustrated double perovskites La_2LiRuO_6 and Ba_2YRuO_6. *Phys. Rev. B,* **2009,** 80, 134423.

(8) Carlo, J. P.; Clancy, J. P.; Fritsch, K.; Marjerrison, C. A.; Granroth, G. E.; Greedan, J. E.; Dabkowska, H. A.; Gaulin, B. D. Spin gap and the nature of the 4d(3) magnetic ground state in the frustrated fcc antiferromagnet Ba_2YRuO_6. *Phys. Rev. B,* **2013,** 88, 024418.

(9) Kermarrec, E.; Marjerrison, C. A.; Thompson, C. M.; Maharaj, D. D.; Levin, K.; Kroeker, S.; Granroth, G. E.; Flacau, R.; Yamani, Z.; Greedan, J. E.; Gaulin, B. D. Frustrated fcc antiferromagnet Ba_2YOsO_6: Structural characterization, magnetic properties, and neutron scattering. *Phys. Rev. B,* **2015,** 91, 075133.

(10) Morrow, R.; Freeland, J. W.; Woodward, P. M. Probing the Links between Structure and Magnetism in $Sr_{2-x}Ca_xFeOsO_6$ Double Perovskites. *Inorg. Chem.,* **2014,** 53, 7983-7992.

(11) Phelan, B. F.; Seibel, E. M.; Badoe, D.; Xie, W. W.; Cava, R. J. Influence of structural distortions on the Ir magnetism in $Ba_{2-x}Sr_xYIrO_6$ double perovskites. *Solid State Commun.,* **2016,** 236, 37-40.

(12) Katz, L.; Ward, R. Structure relations in mixed metal oxides. *Inorg. Chem.,* **1964,** 3, 205.

(13) Thumm, I.; Treiber, U.; Kemmlersack, S. Oxyperovskites with pentavalent and tetravalent iridium compounds of the type $Ba_2B^{3+}Ir^{5+}O_6$ AND $Ba_3B^{3+}IR_2^{4.5+}O_9$. *J. Solid State Chem.,* **1980,** 35, 156-166.

(14) Wakeshima, M.; Harada, D.; Hinatsu, Y. Crystal structures and magnetic properties of ordered perovskites $A_2R^{3+}Ir^{5+}O_6$ (A=Sr, Ba; R=Sc, Y, La, Lu). *J. Alloys Compd. ,* **1999,** 287, 130-136.

(15) Anderson, M. T.; Greenwood, K. B.; Taylor, G. A.; Poeppelmeier, K. R. B-cation arrangements in double perovskites. *Prog. Solid State Chem.,* **1993,** 22, 197-233.

(16) Vasala, S.; Karppinen, M. $A_2B'B''O_6$ perovskites: A review. *Prog. Solid State Chem.,* **2015,** 43, 1-36.

(17) Howard, C. J.; Kennedy, B. J.; Woodward, P. M. Ordered double perovskites - a group-theoretical analysis. *Acta Crystallogr., Sect. B: Struct. Sci.,* **2003,** 59, 463-471.

(18) Cao, G.; Qi, T. F.; Li, L.; Terzic, J.; Yuan, S. J.; DeLong, L. E.; Murthy, G.; Kaul, R. K. Novel Magnetism of $Ir^{5+}(5d^4)$ ions in the Double Perovskite Sr_2YIrO_6. *Phys. Rev. Lett.,* **2014,** 112, 056402.

(19) Panda, S. K.; Bhowal, S.; Li, Y.; Ganguly, S.; Valentí, R.; Nordström, L.; Dasgupta, I. Electronic structure and spin-orbit driven magnetism in $d^{4.5}$ insulator $Ba_3YIr_2O_9$. *Phys. Rev. B,* **2015,** 92, 180403.

(20) de Vries, M. A.; McLaughlin, A. C.; Bos, J. W. G. Valence Bond Glass on an fcc Lattice in the Double Perovskite Ba_2YMoO_6. *Phys. Rev. Lett.,* **2010,** 104, 177202.
(21) Thompson, C. M.; Carlo, J. P.; Flacau, R.; Aharen, T.; Leahy, I. A.; Pollichemi, J. R.; Munsie, T. J. S.; Medina, T.; Luke, G. M.; Munevar, J.; Cheung, S.; Goko, T.; Uemura, Y. J.; Greedan, J. E. Long-range magnetic order in the $5d^2$ double perovskite Ba_2CaOsO_6: comparison with spin-disordered Ba_2YReO_6. *J. Phys.: Condens. Matter,* **2014,** 26, 306003.
(22) Wallwork, K. S.; Kennedy, B. J.; Wang, D. Australian Synchrotron Powder Diffractometer. *AIP Conference Proceedings,* **2007,** 879, 879.
(23) Liss, K. D.; Hunter, B.; Hagen, M.; Noakes, T.; Kennedy, S. Echidna - the new high-resolution powder diffractometer being built at OPAL. *Physica B,* **2006,** 385-86, 1010-1012.
(24) Larson, A. C.; Von Dreele, R. B. *General Structure Analysis System (GSAS)*, Los Alamos National Laboratory Report LAUR 86-748: 1994.
(25) Toby, B. H. EXPGUI, a graphical user interface for GSAS. *J. Appl. Cryst.,* **2001,** 34, 210-213.
(26) Shannon, R. D. Revised effective ionic-radii and systematic studies of interatomic distances in halides and chalcogenides. *Acta Crystallogr. Sect. A,* **1976,** 32, 751-767.
(27) Bader, H.; Kemmlersack, S. On oxygen perovskites with pentavalent ruthenium A_2BRuO_6 with A = Ba, Sr. *Z. Anorg. Allg. Chem.,* **1980,** 466, 97-102.
(28) Kayser, P.; Alonso, J. A.; Mompean, F. J.; Retuerto, M.; Croft, M.; Ignatov, A.; Fernandez-Diaz, M. T. Crystal and Magnetic Structure of Sr_2BIrO_6 (B = Sc, Ti, Fe, Co, In) in the Framework of Multivalent Iridium Double Perovskites. *Eur. J. Inorg. Chem.,* **2015**, 5027-5038.
(29) Velickov, B.; Kahlenberg, V.; Bertram, R.; Bernhagen, M. Crystal chemistry of $GdScO_3$, $DyScO_3$, $SmScO_3$ and $NdScO_3$. *Z. Kristallogr. ,* **2007,** 222, 466-473.
(30) Taylor, A. E.; Morrow, R.; Singh, D. J.; Calder, S.; Lumsden, M. D.; Woodward, P. M.; Christianson, A. D. Magnetic order and electronic structure of the $5d^3$ double perovskite Sr_2ScOsO_6. *Phys. Rev. B,* **2015,** 91, 100406.
(31) Groen, W. A.; Vanberkel, F. P. F.; Ijdo, D. J. W. Dineodymium magnesium titanate (IV) - a Rietveld refinement of neutron powder diffraction data. *Acta Crystallogr., Sect. C: Cryst. Struct. Commun.,* **1986,** 42, 1472-1475.
(32) Zhou, Q. D.; Kennedy, B. J. High-temperature powder synchrotron diffraction studies of synthetic cryolite Na_3AlF_6. *J. Solid State Chem.,* **2004,** 177, 654-659.
(33) Ranjbar, B.; Reynolds, E.; Kayser, P.; Kennedy, B. J.; Hester, J. R.; Kimpton, J. A. Structural and Magnetic Properties of the Iridium Double Perovskites $Ba_{2-x}Sr_xYIrO_6$. *Inorg. Chem.,* **2015,** 54, 10468-10476.
(34) Nagai, I.; Yoshida, Y.; Ikeda, S. I.; Matsuhata, H.; Kito, H.; Kosaka, M. Canted antiferromagnetic ground state in $Sr_3Ir_2O_7$. *J. Phys.: Condens. Matter* **2007,** 19, 136214.
(35) Dey, T.; Maljuk, A.; Efremov, D. V.; Kataeva, O.; Gass, S.; Blum, C. G. F.; Steckel, F.; Gruner, D.; Ritschel, T.; Wolter, A. U. B.; Geck, J.; Hess, C.; Koepernik, K.; van den Brink, J.; Wurmehl, S.; Buchner, B. Ba_2YIrO_6: A cubic double perovskite material with Ir^{5+} ions. *Phys. Rev. B,* **2016,** 93, 014434.
(36) Ranjbar, B.; Pavan, A.; Kennedy, B. J.; Zhang, Z. M. Structural and magnetic properties of the ruthenium double perovskites $Ba_{2-x}Sr_xYRuO_6$. *J. Chem. Soc., Dalton Trans. ,* **2015,** 44, 10689-10699.
(37) Kanungo, S.; Yan, B. H.; Felser, C.; Jansen, M. Active role of nonmagnetic cations in magnetic interactions for double-perovskite Sr_2BOsO_6(B = Y, In, Sc). *Phys. Rev. B,* **2016,** 93, 161116.

For Table of Contents Only

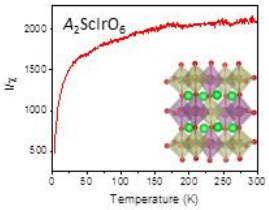

Magnetization measurements show the two Ir(V) perovskite oxides Ba_2ScIrO_6 and Sr_2ScIrO_6 have magnetic moments close to zero as a consequence of strong spin-orbit coupling that results in a $J_{eff} \sim 0$ ground state. Whereas $BaScIrO_6$ has a cubic structure the structure of Sr_2ScIrO_6 is monoclinic, however the tilting induced distortion of the IrO_6 octahedra is insufficient to generate crystal field splitting strong enough to quench the spin orbit coupling.